

Analysis of complex bursting in cortical pyramidal neuron models[☆]

Adam Kepecs*, Xiao-Jing Wang

Volen Center for Complex Systems, Brandeis University, Waltham, MA 02254, USA

Accepted 13 January 2000

Abstract

Burst firing is a prominent feature of cortical pyramidal cells and is thought to have significant functional roles in reliable signaling and synaptic plasticity. Modeling studies have successfully elucidated possible biophysical mechanisms underlying complex bursting in pyramidal cells. Based on these results (Pinsky, Rinzel, *J. Comput. Neurosci.* 1 (1994) 39–60), we have built a simplified two-compartment burst model. Using the fast- and slow-variable analysis method, we show that complex bursting is an instance of square-wave bursting, where the dendritic slow potassium conductance is the single slow variable. The coupling parameters between the two compartments change the topological class of bursting thereby altering the firing patterns of the neuron. These results explain the diverse set of firing patterns seen with different dendritic morphologies (Mainen, Sejnowski, *Nature* 382 (1996) 363–366). © 2000 Elsevier Science B.V. All rights reserved.

Keywords: Phase-plane analysis; Complex burst; Bifurcation diagram

1. Introduction

Pyramidal cells in many cortical areas fire stereotyped bursts of action potentials termed complex spikes or complex bursts. These bursts consist of 2–7 action potentials occurring in a ~ 30 ms window. First observed in hippocampal single-unit extracellular recordings, these were termed ‘complex spikes’ and were later identified by intracellular techniques. Burst firing is thought to play an important role in reliable signaling [5,15] and synaptic plasticity [2].

[☆]This work was partially supported by the NIH and the Alfred P. Sloan Foundation.

*Corresponding author.

E-mail address: adam@volen.brandeis.edu (A. Kepecs).

Modeling studies have determined that these bursting oscillations can be generated by a variety of biophysical mechanisms. The systematic theoretical analysis of bursting was pioneered by Rinzel [10]. Such analysis is useful, since mathematical understanding of various burst patterns have given insights into their biophysical character, their emergence and the switching and resetting of behaviors between different modes of firing [16]. Rinzel classified system variables as either “slow” if they changed little during a single spike but significantly during a burst or “fast” if their primary behavior was determined by a spike. From a theoretical point of view a burst is an action potential waveform made up of a slow and a fast component. The fast component is an autocatalytic type of reaction whereas the slow is a negative feedback to the system. Analyzing a burst requires one to find the right separation of slow and fast subsystems and to map the fast system while holding the slow system constant and treating it as a parameter. Based on these methods several prototypical bursting types have been identified and analyzed (e.g. triangular, square-wave, parabolic and elliptic bursting [1,16]). Complex bursting, however, has not yet been analyzed in this sense [16].

Traub’s 19-compartment model [13] was the first successful modeling attempt to recreate a complex burst. This was followed by Traub [12], a model built with branching morphology for hippocampal cells and Rhodes and Gray [9] for neocortical cells. Intuitive understanding of these models came from Pinsky and Rinzel [8], who reduced Traub’s model to a two-compartment model that captures the essence of bursting by the spatial segregation of fast and slow currents. Mainen and Sejnowski [6] showed how certain parameter variations can be understood as changing morphology which then translate the various known firing patterns from different locations of the parameter space into morphological space. Here, we introduce an even more simplified, minimal two-compartment model for complex bursting. Using this model we show, following Rinzel’s method, how this type of bursting emerges in the framework of dynamical systems.

2. Methods

Our model includes only the minimal biophysical mechanisms necessary to study the phenomenon of complex bursting [3]. Following Pinsky and Rinzel [8], we represent the perisomatic region with a single compartment and the dendrites lumped into another. The somatic compartment includes only the channels necessary for spike generation (I_{Na} and I_K) while the dendritic compartment includes a slow potassium I_{KS} and a persistent sodium I_{NaP} current. The membrane potential follows the equations below:

$$C_m \frac{dV_s}{dt} = -I_{Na} - I_K - I_{Leak} - \frac{g_c}{p} (V_s - V_d) + I_{soma}, \quad (1)$$

$$C_m \frac{dV_d}{dt} = -I_{NaP} - I_{KS} - I_{Leak} - \frac{g_c}{(1-p)} (V_d - V_s) + I_{dendrite}, \quad (2)$$

where I_{soma} and I_{dendrite} are current injections to the compartments. The voltage-dependent conductances are described using standard Hodgkin–Huxley formalism. $I_{\text{Na}} = g_{\text{Na}} m_{\text{ss}}^3 h (V - E_{\text{Na}})$, with $\alpha_m = -0.1(V + 31)/(\exp(-0.1(V + 31)) - 1)$, $\beta_m = 4 \exp(-(V + 56)/18)$; $\alpha_h = 0.07 \exp(-(V + 47)/20)$, and $\beta_h = 1/(\exp(-0.1(V + 17)) + 1)$. $I_{\text{K}} = g_{\text{K}} n^4 (V - E_{\text{K}})$, with $\alpha_n = -0.01(V + 34)/(\exp(-0.1(V + 34)) - 1)$, and $\beta_n = 0.125 \exp(-(V + 44)/80)$. $I_{\text{NaP}} = g_{\text{NaP}} m_{\text{ss}}^3 (V - E_{\text{Na}})$, $m_{\text{ss}}(V) = 1/(1 + \exp(-(V + 57.7)/7.7))$. $I_{\text{KS}} = g_{\text{KS}} q (V - E_{\text{K}})$, with $q_{\text{ss}}(V) = 1/(1 + \exp(-(V + 35)/6.5))$ and $\tau_q(V) = 200/(\exp(-(V + 55)/30) + \exp((V + 55)/30))$. $I_{\text{Leak}} = g_{\text{Leak}} (V - E_{\text{Leak}})$, $C_m = 1 \mu\text{F}/\text{cm}^2$. The coupling conductance is varied, the base value is $g_c = 1 \text{ mS}/\text{cm}^2$. The asymmetry between the areas of the two compartments is taken into account in the parameter $p = \text{somatic area}/\text{total area}$ which has a base value of 0.15. The temperature scaling factors are $\phi_m = 10$, $\phi_h = \phi_n = 3.33$. Other parameter values are: $g_{\text{Leak}} = 0.18$, $g_{\text{NaP}} = 0.12$, $g_{\text{KS}} = 0.7$, $g_{\text{Na}} = 55$, $g_{\text{K}} = 20$ (in mS/cm^2); $E_{\text{Leak}} = -65$, $E_{\text{Na}} = +55$, $E_{\text{K}} = -90$ (in mV).

Altogether the model consists of five differential equations. Simulations were performed using MATLAB, XPP and AUTO for bifurcation analysis.

3. Results

3.1. Firing patters

The basic bursting behavior of the model is shown in Fig. 1A. By increasing the injected current, bursting gives way to spiking (Fig. 1C). Note that repetitive spiking appears via a chaotic parameter region shown on Fig. 1B. The Poincaré map of Fig. 1B is a tent map, indicative of square-wave bursting [11,14]. In similar models [8,6] a range of firing behaviors were found by modifying the coupling parameters. When the coupling strength, g_c , is strong, the burst gets progressively shorter, changing into doublets and finally to single spikes (Fig. 1D). Note that this type of single spike shows after-depolarization instead of after-hyperpolarization.

When the two compartments are weakly coupled (e.g., $g_c = 0.1$), the bursts take on an entirely different shape; the dendritic voltage does not fully follow somatic events, showing only a small hump during a burst (Fig. 1E). The interspike intervals during this burst show a parabolic pattern, hence this kind of burst has been called nearly-parabolic burst [7]. For larger current injections the bursting disappears (Fig. 1F). Spiking is now modulated in frequency by the slow dendritic depolarizations and the instantaneous frequency is nearly sinusoidal. This type of firing might be called *nearly parabolic spiking*.

By decreasing the relative area of the dendritic compartment (increasing p), the model can be switched to spike-train adaptation. The degree of adaptation is greater with larger relative somatic area (compare Fig. 1G and 1H, with $p = 0.2$ and 0.6 respectively).

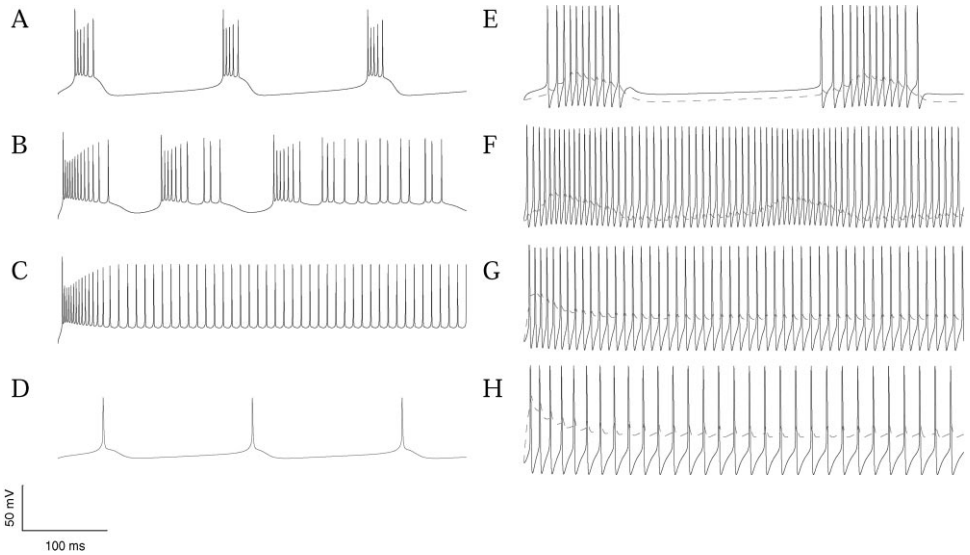


Fig. 1. Various firing patterns exhibited by the model. For A–B the somatic voltage is plotted; for E–F dendritic voltage is also plotted with dashed lines. Each trace was produced by using following parameter triplets (g_c, p, I_{soma}) A (1, 0.15, 3), B (1, 0.15, 19.7), C (1, 0.15, 23), D (5, 0.15, 3), E (0.1, 0.15, 7), F (0.1, 0.15, 20), G (0.1, 0.2, 15), H (0.1, 0.6, 30).

3.2. Phase-plane analysis

During a burst I_{KS} increases gradually, building up with each spike. In the dendrites, the electrotonic current spreading from the soma is a major determinant of voltage; it initiates the burst. I_{KS} receives help from the leak conductance. In the soma, electrotonic current from the dendrites is significant after a spike and initiates the subsequent somatic spike. The burst terminates when due to the buildup of I_{KS} the dendritic compartment goes below threshold.

In order to look at the dynamics of the system, we first calculated the bifurcation diagram of the fast subsystem with respect to the slow variable q , the activation gate of I_{KS} . The somatic potential is a good representative of the fast subsystem. The equilibrium states appear as a Z-shaped manifold (Fig. 1A). As q increases, it becomes unstable at a supercritical Hopf bifurcation. The resulting periodic solution is plotted as the maxima, minima (thick) and average membrane potential (dash-dotted) within a burst (Fig. 2). The periodic solution disappears at a homoclinic bifurcation. There is a bistable regime where a stable resting and a periodic solution coexist. In order to see where the actual burst is confined within this phase-plane, the somatic potential is plotted against q of I_{KS} in the full system. We see the typical, computationally mutated, many-eared “cat on a plane” emerging in the bistable regime. Now, the question becomes whether we can account for the dynamics of q within this diagram. The slow nullcline of dq/dt intersects the unstable fixed solution within the bistable

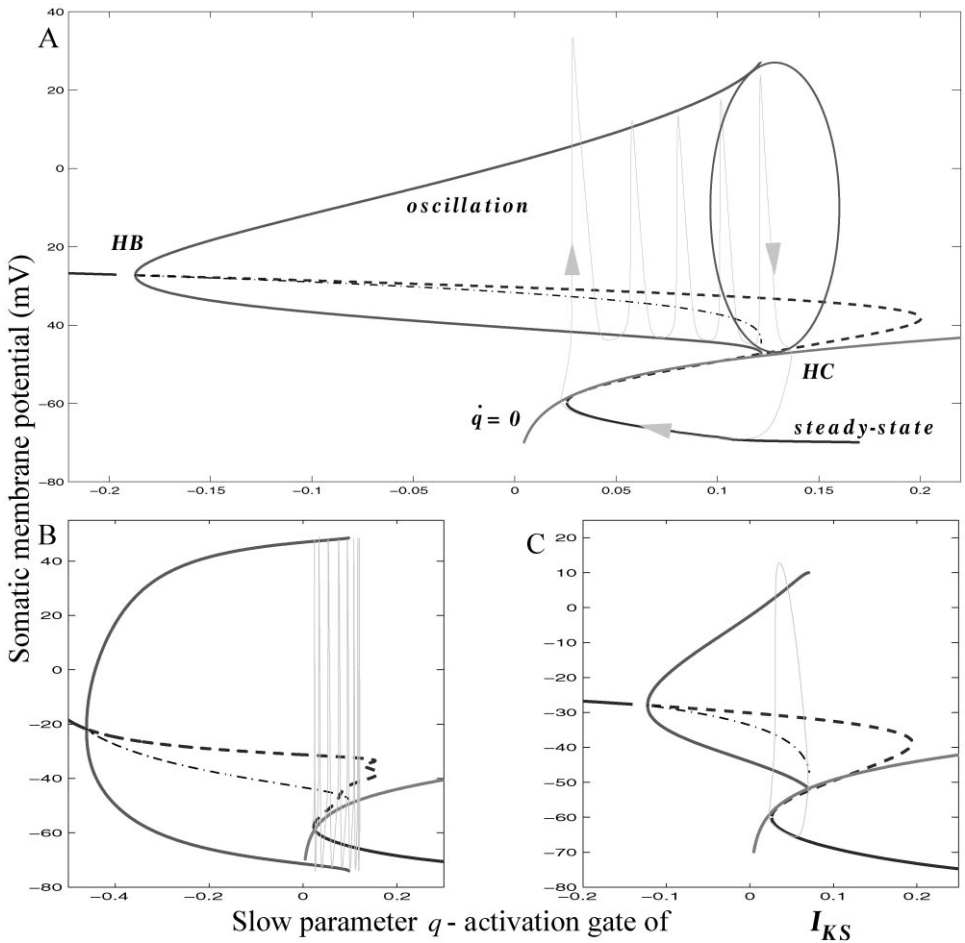


Fig. 2. Bifurcation diagram A ($g_c = 1$). The Z-shaped steady-state (solid) becomes unstable (dashed). The thick cone is the periodic solution. The average membrane potential is dash-dotted. The temporal evolution of (q, V_s) pairs of a burst is shown with arrows. The $dq/dt = 0$ nullcline crosses just above the left knee. B Same with weak coupling, $g_c = 0.1$ and C Strong coupling, $g_c = 5$.

states. Along this curve the value of q does not change. Above this ($dq/dt > 0$) q increases, below this ($dq/dt < 0$) q decreases. Since $dq/dt < 0$ at the lower stable branch, it moves leftward until it hits the left knee of the Z-curve and switches via a saddle-node bifurcation to the periodic solution. As the phase-point is now above the nullcline it moves rightward, oscillating with greater amplitude and longer period until it hits the middle branch of the slow manifold returning to the resting stable state. Here it is below the nullcline and works its way back toward the left knee. Note that the burst terminates at an infinite period orbit, translating into growing

interspike intervals within the burst. The q variable is moved by the average potential or in biophysical terms the slow potassium conductance gets slowly activated by the voltage over time. Since the entire periodic solution is above the nullcline the average does the same.

When the two compartments are only weakly coupled a different picture emerges (Fig. 2B). The periodic solution's lower branch is below the rest state and spikes "undershoot". However, the average voltage is still above the nullcline thus bursting remains. The Z-curve is slightly deformed at the right knee where there is a Hopf bifurcation. At greater coupling strengths the bistable region gradually shrinks. At $g_c = 5$, the periodic solution vanishes after a single spike (Fig. 2C). Since the phase-point gets back to the resting state at once, there is no undershoot or after hyperpolarization.

4. Discussion

By determining the exact mechanisms of bursting one can gain insights into an array of firing behaviors and the nature of transitions between them. This understanding can facilitate the study of how different factors might influence firing patterns. We found that the complex bursting is a form of square-wave bursting (Fig. 2A). This requires a single slow variable which in our case is the slowly activating dendritic potassium channel, I_{KS} . The burst occurs in a bistable region, thus it can be reset by brief stimuli. The different modes of behavior in this model are explained by the way coupling changes the bifurcation diagram (Figs. 2B and C) that is how the slow subsystem is coupled to the fast, spiking subsystem. Adjusting the coupling strength, g_c , and the relative area, p , switches the model among the following types of firing behaviors: bursting, regular spiking, spikes with after-depolarization, parabolic bursting, sinusoidal spiking and spike adaptation (Fig. 1).

What are the functional implications of this? Factors that influence the coupling can dramatically change the firing behavior of a complex bursting cell. The idea that morphology has a major influence on firing behavior rests on the assumption that different types of currents are segregated along morphological boundaries. The results of Mainen and Sejnowski [6] can be now seen in the structure of the bifurcation diagrams (Fig. 2). In addition, this predicts that factors changing the dendritic slow potassium current could also change bursting behavior. For example if dendritic inhibition modulates the slow potassium current, the shape of the burst is affected [4]. Specialized actions of differently localized inhibitory synapses may also be explained by this result. As dendritic inhibition changes the speed of the slowly varying parameter q , it modulates the burst pattern. Somatic inhibition, on the other hand can only stop or delay the burst [4] but has no access to q to modify the burst waveform. In summary, complex bursting is a special case of square-wave bursting where the compartmental segregation of fast and slow systems enables physiological manipulations to dramatically change firing behavior.

References

- [1] R. Bertram, M.J. Butte, T. Kiemel, A. Sherman, *Bull. Math. Biol.* 57 (3) (1995) 413–439.
- [2] P.T. Huerta, J.E. Lisman, *Neuron* 15 (5) (1995) 1053–1063.
- [3] A. Kamondi, L. Acsády, X.-J. Wang, Gy. Buzsáki, *Hippocampus* 8 (3) (1998) 244–260.
- [4] Á. Kepecs, P. Érdi, *CNS '97, Proceedings*, 1997, p. 79.
- [5] J.E. Lisman, *TINS* 20 (1) (1997) 38–43.
- [6] Z.F. Mainen, T.J. Sejnowski, *Nature* 382 (1996) 363–366.
- [7] M. Pernarowsky, *SIAM J. Appl. Math.* 54 (3) (1994) 814–832.
- [8] P.F. Pinsky, J. Rinzel, *J. Comput. Neurosci.* 1 (1994) 39–60.
- [9] P.A. Rhodes, C.M. Gray, *Neural Comput.* 6 (1994) 1086–1110.
- [10] J. Rinzel, in: E. Teramoto, M. Yamaguti (Eds.), *Mathematical Topics in Population Biology, Morphogenesis and Neuroscience*, Lecture Notes in Biomathematics, Vol. 71, Springer, Berlin, 1987, pp. 267–281.
- [11] D. Terman, *SIAM J. Appl. Math.* 51 (5) (1991) 11418–11450.
- [12] R.D. Traub, J.G.R. Jefferys, R. Miles, M.A. Whittington, K. Tóth, *J. Physiol.* 481 (1994) 79–95.
- [13] R.D. Traub, R.K.S. Wong, R. Miles, H. Michelson, *J. Neurophysiol.* 66 (1991) 635–650.
- [14] X.-J. Wang, *Physica D (Special Issue on Homoclinic Chaos)* 62 (1993) 263–274.
- [15] X.-J. Wang, *Neuroscience* 89 (1999) 347–362.
- [16] X.-J. Wang, J. Rinzel, in: M. Arbib (Ed.), *The Handbook of Brain Theory and Neural Networks*, MIT Press, Cambridge, MA, 1995, pp. 686–691.